Biochimica et Biophysica Acta 1808 (2011) 2477–2487

Contents lists available at ScienceDirect

Biochimica et Biophysica Acta

journal homepage: www.elsevier.com/locate/bbamem

The hERG K^+ channel S4 domain L532P mutation: Characterization at 37 °C

Yi H. Zhang [a], Charlotte K. Colenso [b], Richard B. Sessions [b], Christopher E. Dempsey [b], Jules C. Hancox [a,*]

[a] School of Physiology and Pharmacology and Cardiovascular Research Laboratories, Medical Sciences Building, University of Bristol, University Walk, Bristol BS8 1TD, UK
[b] School of Biochemistry, Medical Sciences Building, University of Bristol, University Walk, Bristol BS8 1TD, UK

ARTICLE INFO

Article history:
Received 4 May 2011
Received in revised form 28 June 2011
Accepted 6 July 2011
Available online 14 July 2011

Keywords:
Arrhythmia
Dronedarone
hERG
I_{Kr}
Short QT syndrome
Potassium channel

ABSTRACT

hERG (*human Ether-à-go-go Related Gene*) is responsible for ion channels mediating rapid delayed rectifier potassium current, I_{Kr}, which is key to cardiac action potential repolarization. Gain-of-function *hERG* mutations give rise to the SQT1 variant of the Short QT Syndrome (SQTS). Reggae mutant zebrafish, with a S4 *zERG* mutation (Leucine499Proline; L499P), display arrhythmic features analogous to those seen in the SQTS. The affected S4 domain ERG residue is highly conserved. This study was executed to determine how the homologous hERG mutation (L532P) influences channel function at 37 °C. Whole-cell measurements of current (I_{hERG}) were made from HEK 293 cells expressing WT or L532P hERG. The half maximal activation voltage ($V_{0.5}$) of L532P I_{hERG} was positively shifted by ~+36 mV compared to WT I_{hERG}; however at negative voltages a pronounced L532P I_{hERG} was observed. Both activation and deactivation time-courses were accelerated for L532P I_{hERG}. The inactivation $V_{0.5}$ for L532P I_{hERG} was shifted by ~+32 mV. Under action potential (AP) voltage-clamp, L532P I_{hERG} exhibited a dome-shaped current peaking at ~+16 mV, compared to ~−31 mV for WT-I_{hERG}. The L532P mutation produced an ~5-fold increase in the IC_{50} for dronedarone inhibition of I_{hERG}. Homology modeling indicated that the L532 residue within the S4 helix lies closely apposed to the S5 region of an adjacent hERG subunit. Alterations to the S4 domain structure and, potentially, to interactions between adjacent hERG subunits are likely to account for the functional effects of this mutation.

1. Introduction

The cardiac rapid delayed rectifier potassium channel passes ionic current (I_{Kr}) that plays an important role in cardiac action potential (AP) repolarization [1,2]. The pore-forming subunit of I_{Kr} channels is encoded by *human Ether-à-go-go-Related Gene* (*hERG*; alternative nomenclatures *KCNH2* or Kv11.1) [3,4]. Loss-of-function hERG mutations are responsible for the LQT2 variant of congenital long QT syndrome (LQTS), while unique structural features of the hERG channel render it highly susceptible to pharmacological blockade and make it an important target for antiarrhythmic drugs and drugs associated with the acquired form of the LQTS [2,5–7].

Within the last decade the hERG channel has also been implicated in the genetic 'short QT syndrome' (SQTS), a condition characterized by abbreviated QT intervals, poor rate adaptation of the QT interval and an increased susceptibility to both atrial and ventricular arrhythmias and to sudden death [8,9]. The first variant of the SQTS to be genotyped (SQT1) was found to be caused by base substitutions leading to a single amino-acid change (Asn588Lys; 'N588K') in the S5-Pore linker of the hERG channel [10,11]. Detailed electrophysiological analysis of N588K-hERG showed the dominant effect of the mutation to be a marked right-ward shift (by ~+60 to +90 mV) in the voltage-dependence of inactivation of hERG current (I_{hERG}), leading to substantially increased current during the repolarizing phases of both ventricular and atrial APs [10,12–14]. Due to its markedly altered inactivation properties, the N588K hERG mutant also exhibits markedly reduced sensitivity to Class III antiarrhythmic I_{Kr} inhibitors (sotalol, E-4031), with much less of an attenuation of the effect of Class Ia drugs (quinidine, disopyramide) [10,15,16]. A second SQT1 hERG channel gain-of-function pore mutation (Thr618Ile; 'T618I' located in the channel pore-helix), which also exhibits modified inactivation kinetics, has recently been reported [32]. There is no genetically accurate mammalian model of SQT1; consequently, efforts to understand the basis of arrhythmogenicity in this form of the SQTS have relied either on computer modeling (e.g. [17–20]) or upon the application of K^+ channel openers to tissue preparations [21–24].

The only existing vertebrate genetic model of a hERG-linked SQTS-like arrhythmogenic syndrome is the zebrafish Reggae mutant [25]. Reggae mutant zebrafish embryos exhibit action potential abbreviation, cardiac fibrillation and intermittent cardiac arrest, while adult fish exhibit shorted QT_c intervals [25]. Positional cloning has identified the mutation responsible as residing in exon 8 of the zebrafish ERG channel (zERG) [25]. A leucine to proline substitution (L499P) was found in the S4 (voltage-sensor) region of zERG. This region is highly conserved across species (Fig. 1A and see [25]) with

* Corresponding author. Tel.: +44 117 3312292; fax: +44 117 331 2288.
E-mail address: Jules.hancox@bristol.ac.uk (J.C. Hancox).

0005-2736 © 2011 Elsevier B.V. Open access under CC BY-NC-ND license.
doi:10.1016/j.bbamem.2011.07.001

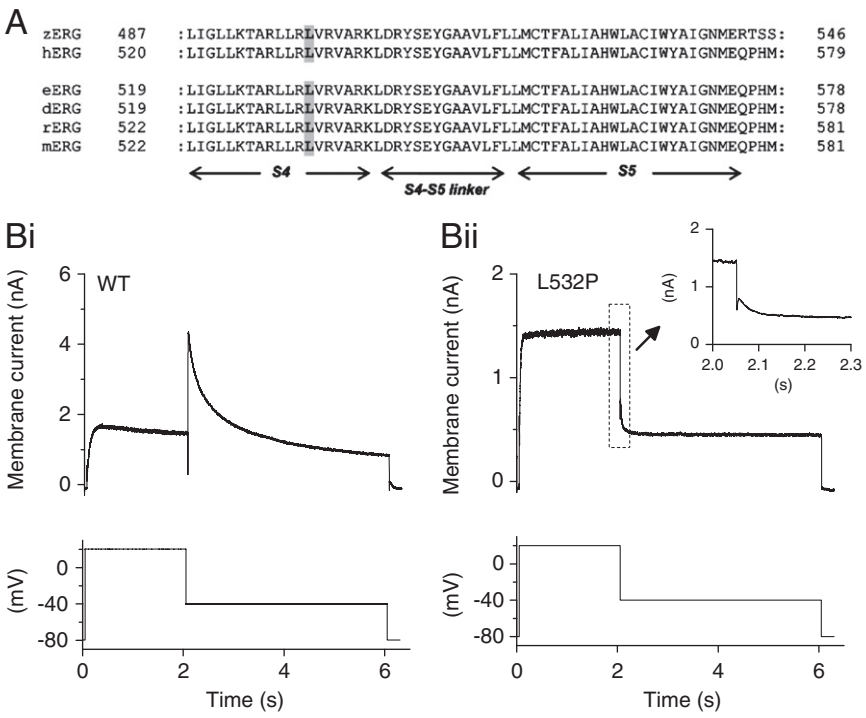

Fig. 1. (A) Amino acid sequence alignment for region encompassing zebrafish (zERG) L499 with human (hERG), horse (eERG), dog (dERG), rat (rERG) and mouse (mERG). Domains S4, S5 and the S4–S5 linker are indicated below the sequences. The L at position 532 of hERG is highly conserved across species and is highlighted in gray. (B) Example current traces for WT (upper panel of Bi) and mutant L532P I_{hERG} (upper panel of Bii) with corresponding voltage protocol used shown in the lower panels. Note that the current scales in Bi and Bii differ. Inset to Bii shows higher gain representation of L532P tail current.

the equivalent mutation to hERG being L532P. Electrophysiological analysis of L499P zERG and L532P hERG in *Xenopus* oocytes has shown gain-of-function kinetic effects of the mutation, with alterations to activation and inactivation voltage-dependence over physiologically relevant membrane potentials [25]. Due to the fact that the L532 residue is located in a different segment of the channel to those in which the N588 and T618 residues reside, detailed information on the nature of the distinct kinetic changes produced by the L532P hERG mutation and its net effect on repolarizing current profile would provide valuable comparative information to that presently available for these human short QT hERG mutations. The kinetics of I_{hERG} have been shown to exhibit a complex temperature dependence, making it difficult to extrapolate directly results obtained at ambient temperature to human body temperature [26]; properties of recombinant hERG channels also appear to be closest to those of native I_{Kr} when channels are expressed in a mammalian cell line and studied at human body temperature [2,27]. Consequently, the present study was undertaken to determine the effects of the L532P mutation on I_{hERG} recorded from mammalian cells at 37 °C. Our results: (i) constitute quantitative information on the effects of the L532P mutation on both voltage and time-dependent kinetics of I_{hERG}; (ii) demonstrate the ability of this mutation to alter the hERG channel's sensitivity to pharmacological inhibition and (iii) indicate the structural context for the affected amino-acid residue of the channel.

2. Material and methods

2.1. Mutagenesis

The L532P hERG mutation was generated using the QuickChange® site-directed mutagenesis kit (Stratagene, La Jolla, CA). In brief, a pair of complementary oligonucleotide primers containing the mutation (forward primer sequence 5′CTGCTGCGGCCGGTGCGCGTG3′ and reverse primer sequence 5′CACGCGCACCGGCCGCAGCAG3′, synthesized by Sigma-Genosys, Haverhill, UK) was used in a PCR reaction (95 °C for 1 min, 60 °C for 1 min, 68 °C for 16 min for 18 cycles) by using hERG in a modified pcDNA3.0 vector as a DNA template. A DpnI digest of the PCR mix was then performed for 1 h at 37 °C. Competent DH5α *Escherichia coli* (Invitrogen, Paisley, UK) were transformed using standard procedures. The mutation was confirmed by sequencing of the entire open reading frame (Eurofins MWG Operon, Ebersberg, Germany).

2.2. Cell culture and transfection

HEK 293 cells (European Collection of Cell Cultures, Porton Down, UK) were maintained at 37 °C, 5% CO_2 in Dulbecco's minimum essential medium with Glutamax-1 (DMEM; Gibco, Paisley, UK). This was supplemented with 10% fetal bovine serum, 50 μg ml^{-1} gentamycin (Gibco, Paisley, UK). Cells were transiently transfected with cDNA plasmids encoding WT and mutant hERG using Lipofectamine LTX (Invitrogen, Paisley, UK) according to the manufacturer's instructions. Expression plasmid encoding CD8 was also added (in pIRES, donated by Dr I Baró, University of Nantes, France) to be used as a successful marker of transfection. Recordings were performed 12–72 h after transfection. Successfully transfected cells (positive to CD8) were identified using Dynabeads® (Invitrogen, Paisley, UK).

2.3. Solutions for electrophysiological recordings

Once in the recording chamber, cells were superfused with normal Tyrode's containing (in mM): 140 NaCl, 4 KCl, 2.5 $CaCl_2$, 1 $MgCl_2$, 10 Glucose, and 5 HEPES (titrated to pH of 7.45 with NaOH). Patch-pipettes were fire-polished to 2.5–4 MΩ. The pipette dialysis solution for I_{hERG} measurement contained (in mM): 130 KCl, 1 $MgCl_2$, 5 EGTA, 5 MgATP, and 10 HEPES (titrated to pH of 7.2 with KOH). Dronedarone powder (Sequoia Research Products, Pangbourne, UK) was dissolved in ethanol to produce an initial stock solution of 50 mM, which was serially diluted to produce stock solutions ranging from 50 mM to 3 μM; these were diluted 1:1000 fold with Tyrode's solution to achieve the final superfusate drug concentrations stated in the 'Results'.

2.4. Experimental protocols and analysis

Whole cell conventional and human action potential (AP) voltage clamp recordings of hERG current (I_{hERG}) were made at 37 ± 1 °C as previously reported [33]. Data digitization rates were 10–25 kHz during all protocols and an appropriate bandwidth of 2–10 kHz was set on the amplifier. Note that L532P I_{hERG} exhibited considerable cell-to-cell heterogeneity in amplitude, presumably due to variable transfection efficiency; consequently in a number of figures WT and L532 I_{hERG} are displayed with different current scales (this is highlighted in the relevant figure legends). Statistical comparisons were made using a Student's *t*-test or two way analysis of variance (ANOVA) followed by Tukey post hoc test, as appropriate. *P* values of less than 0.05 were taken as being statistically significant.

2.5. Concentration–response data correction for I_{hERG} run-down

As previously reported [29], in this study dronedarone exhibited a progressive development of I_{hERG} blockade, reaching a stable level of block by 10 min of drug exposure. During this period, there was some overlying run-down of I_{hERG}. Therefore, control experiments were performed. For these, WT and L532P I_{hERG} were monitored during a 2–4 min stabilization period by repeated use of the standard voltage 'step' protocol, followed by a 10 min recording period in normal Tyrode's solution. The mean level of run-down of WT I_{hERG} tails over 10 min was 13.4 ± 1.6% of the peak tail magnitude (n = 6 cells) while for L532P I_{hERG} tails this was 15.7 ± 2.5% (n = 6 cells). To correct concentration–response data for I_{hERG} run-down, we subtracted 13.4% of WT or 15.7% of L532P current magnitude from the last tail current in the control periods and used the resulting value to calculate fractional block following (10 min) exposure to dronedarone.

2.6. Homology modeling

A full open-state homology model of the hERG membrane domain was constructed using the crystal structure of a Kv1.2/Kv2.1 paddle chimera (PDB ID: 2R9R) determined by Long et al [35]. The template was retrieved from the RCSB Protein Data Bank as a monomer. ClustalW2, TMPred and UNIPROT were used to perform the sequence alignment, which was refined manually with the help of literature regarding hERG and other Kv channels. Full details of the model will be described elsewhere; however the homology used to align the S4 sequence of hERG into the paddle chimera structure is shown in Fig. 7. Amino acid substitutions, including generation of the L532P mutation, were made using the Biopolymer function within InsightII (Accelrys), and the Protein Data Bank was used to search for suitable linker constructs including the extracellular turret region. The symmetry operator within the PDB file 2R9R was used to construct a homotetramer and hERG monomers were superimposed onto this to generate a tetrameric homology model of hERG. The final open channel hERG homology model and the L532P mutant were energy minimized using Discover 2.9.8 (Accelrys). The stereochemical quality of the structures was verified using PROCHECK [49].

3. Results

3.1. Effects of the L532P mutation on I_{hERG} profiles during a standard voltage 'step' protocol

Fig. 1B shows profiles of WT and L532P I_{hERG} elicited by a protocol composed of depolarizing voltage commands from −80 to +20 mV and a repolarizing step to −40 mV. WT I_{hERG} (Fig. 1Bi) exhibited well-established characteristics: current development during the applied depolarization, with a larger I_{hERG} 'tail' elicited during a repolarizing step to −40 mV (end pulse current was 0.48 ± 0.04 fold that of tail current amplitude; n = 14 cells). By contrast L532P I_{hERG} increased rapidly on step-depolarization, with current during the +20 mV step that was much larger than the I_{hERG} tail on repolarization to −40 mV (Fig. 1Bii; end pulse current amplitude was 1.45 ± 0.09 fold that of tail current amplitude; n = 43 cells). Tail current decline was much faster for L532P than for WT I_{hERG} (compare Fig. 1Bii (and inset) with Fig. 1Bi).

The voltage-dependence of WT and L532P I_{hERG} was compared using 2 s depolarizing voltage steps from −80 mV to potentials between −40 and +60 mV. Representative traces are shown in Fig. 2A and B for WT and L532P hERG respectively. WT I_{hERG} increased progressively with depolarization up to ~0 mV, declining at more positive potentials, giving rise to marked negative slope in the current–voltage (I–V) relation (Fig. 2A, C). Proportionately greater L532P than WT I_{hERG} was elicited by depolarization to −40 and −30 mV, but then smaller increases in current were seen with progressive depolarization up to 0–+10 mV (Fig. 2B, C). Rectification of L532P I_{hERG} was evident at positive voltages. The normalized mean I–V data shown in Fig. 2C show the more gradual increase in L532P than WT I_{hERG} up to ~0–+10 mV and positively shifted rectification of the end pulse I–V relationship. Normalized I–V relations for I_{hERG} tail currents were used to compare voltage dependent activation of the two channels, with Boltzmann fitting used to derive half-maximal activation voltage ($V_{0.5}$) and slope (k) values. At −40 mV there was significantly greater L532P I_{hERG} activation than for WT-hERG; however at potentials between −20 mV and ~+30 mV, activation was significantly less extensive for mutant than WT channels, with a shallower slope of the activation relationship (Fig. 2D). Derived $V_{0.5}$ and k values for WT I_{hERG} were −16.6 ± 2.3 mV and 6.8 ± 0.3 mV (n = 7), while for L532P these were +19.2 ± 2.8 mV and 12.4 ± 0.9 mV (n = 9, $P<0.001$ for both $V_{0.5}$ and k versus WT). Thus, L532P hERG showed greater activation than WT I_{hERG} but an ~+36 mV shift in activation $V_{0.5}$ compared to the WT channel.

3.2. Effects of the L532P mutation on the fully activated I–V relation and on deactivation and activation time-courses

The protocol used to elicit the fully activated I–V relation and quantify deactivation (identical to that used previously in [13,31]) is shown in Fig. 3Aii, with representative current traces for WT I_{hERG} in Fig. 3Ai and for L532P I_{hERG} in Fig. 3B. For both channels, the peak current on the repolarizing steps to different voltages was normalized to the maximal observed peak current during the protocol and plotted against voltage [13,31], see Fig. 3C. For WT I_{hERG}, the fully activated I–V relation was maximal for the repolarizing step to ~−30 mV, whereas for L532P I_{hERG} this was positively shifted. The WT hERG fully activated I–V relation reversed at −84.3 ± 0.9 mV (n = 6), whereas the comparable value for L532P was −80.3 ± 0.8 mV (n = 9; $P<0.005$). The deactivating component of I_{tails} at each repolarization step was fitted with a bi-exponential function to derive fast and slow (τ_f and τ_s) time constants of deactivation (plotted in Fig. 3D and E). Both τ_f and τ_s values were significantly smaller for L532P I_{hERG} than for WT I_{hERG} at repolarization potentials of -60 mV and more positive. There were also significant differences between WT and L532P hERG at most membrane potentials examined for the fraction of deactivation described by τ_f (Fig. 3F). An additional observation was that, while bi-exponential fits to deactivating WT I_{hERG} tails yielded little residual unfitted current at negative voltages (for example, residual unfitted components of only 3.4 ± 1.0% and 3.2 ± 0.8% of peak tail current were obtained respectively at −60 and −70 mV), for L532P substantial residual current remained. Thus at −60 mV residual unfitted current for L532P I_{hERG} was 23.4 ± 4.9% of peak tail current ($P<0.01$ compared to WT), although at −70 mV the greater residual I_{hERG} for L532P-hERG (12.4 ± 4.6% of peak tail current) did not attain statistically significant difference from WT hERG ($P>0.05$). The presence of residual current is consistent with greater current activation at some negative voltages for L532P hERG (see also Fig. 2D), though perhaps not with complete destabilization of closed channel state(s). An envelope of tails protocol (inset of Fig. 3G; see also

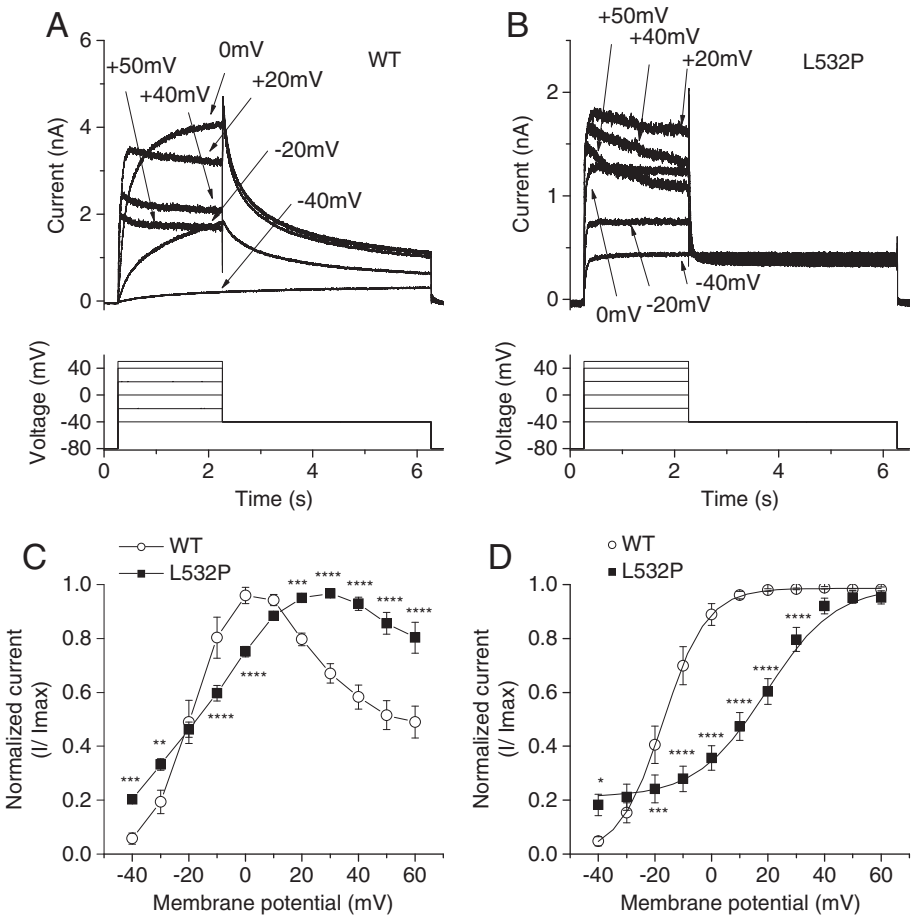

Fig. 2. Current–voltage (I–V) relationship for WT and L532P I_{hERG}. (A, B) Upper panels show representative families of currents from WT hERG (A) and L532P hERG (B), elicited by the voltage protocol shown in the lower panel (start-to-start interval of 12 s between successive voltage steps). For clarity only selected sweeps are shown; note that the current scales in A and B differ. (C) Mean I–V relations for end-pulse current (n = 7 for WT and n = 9 for L532P). (D) Mean normalized tail current I–V relations; for each of WT (n = 7) and L532P (n = 9) data were normalized to the maximal current recorded during the protocol. (* denotes statistic significance of $P<0.05$, ** of $P\leq0.01$, *** of $P\leq0.005$, **** of $P\leq0.001$).

[33]) was used to compare time-dependence of activation of I_{hERG} between the two channels at +20 mV. Mono-exponential fitting of mean normalized tail currents elicited by the protocol (Fig. 3G) yielded for WT I_{hERG} a τ_{act} of 67.9 ± 6.1 ms (n = 9) and of 32.6 ± 2.2 ms for L532P I_{hERG} (n = 6, $P<0.001$). Additional analysis of pulse currents elicited by the I–V protocol shown in Fig. 2A, B between −40 and 0 mV yielded significantly reduced values for time to half-maximal current (t_{half}) at each potential for L532P (at -30 mV t_{half} was 30 ± 10 ms for L532P I_{hERG} compared to 490 ± 30 ms for WT I_{hERG}, $P<0.001$; while at 0 mV the respective values were 10 ± 2 ms and 130 ± 40 ms, $P<0.01$). Collectively, these results indicate that, over a range of potentials, L532P I_{hERG} both activated and deactivated faster than did WT I_{hERG}

3.3. Effects of the L532P mutation on voltage and time dependence of inactivation

The voltage-dependence of WT I_{hERG} inactivation (availability) was assessed using the protocol shown in Fig. 4A (and lower trace in 4 C): an initial step to +40 mV activated and then inactivated I_{hERG}; a 'ladder' of brief (2 ms) repolarizing steps to a range of potentials (to relieve inactivation to varying extents) was followed by a third step to +40 mV. The magnitude of peak current elicited by the third step reflected the extent of availability induced by the second step. Representative WT I_{hERG} records are shown in Fig. 4C. In order to correct for possible deactivation during this protocol, as in previous work from our laboratory [13], a method described by Zou et al [52] was used: peak current amplitudes during the third pulse were obtained by single exponential fitting of the currents and extrapolation to the start of the third step. Peak currents during the third step were then normalized to maximal current and mean data were plotted as shown in Fig. 4E. Boltzmann fitting this relation yielded an inactivation $V_{0.5}$ value of −70.3 ± 1.7 mV (k = 19.6 ± 0.5 mV; n = 9). As rectification of the I–V relation for L532P I_{hERG} in Fig. 2C was positively shifted, in order to ensure adequate inactivation during the availability protocol, the protocol was modified so that the first and third step potential was set to +80 mV (Fig. 4B, lower trace in 4D; see [13]). Representative traces are shown in Fig. 4D with mean normalized data shown in Fig. 4E. Boltzmann-fitting of this plot gave an inactivation $V_{0.5}$ for L532P I_{hERG} of −38.7 ± 3.7 mV (k = 28.7 ± 2.8 mV, n = 6, $P<0.0001$ for $V_{0.5}$ and $P<0.005$ for k value compared with WT). Calculation of the steady-state activation-inactivation parameter product ("window current") across a wide range of voltages (−80 mV to +60 mV) for WT and L532P I_{hERG} indicated slightly greater window current for L532P than WT I_{hERG} at potentials negative to approximately -50 mV and much greater window current for L532P hERG positive to approximately −5 mV (data not shown). The currents elicited following the repolarizing step to -140 mV were also used to quantify the time-course of development of inactivation (from a single-exponential fit) for the two channels; the τ-values obtained for WT and L532P I_{hERG} were 1.34 ± 0.13 ms and 1.0 ± 0.06 ms respectively ($P>0.05$). The rate of recovery from inactivation was assessed using the protocol shown in the inset of Fig. 4F and see [14,34]. Normalized peak outward transient currents were plotted against the duration of the repolarization step and fitted with a mono-exponential function, giving τ values of 1.92 ± 0.07 ms for WT (n = 10)

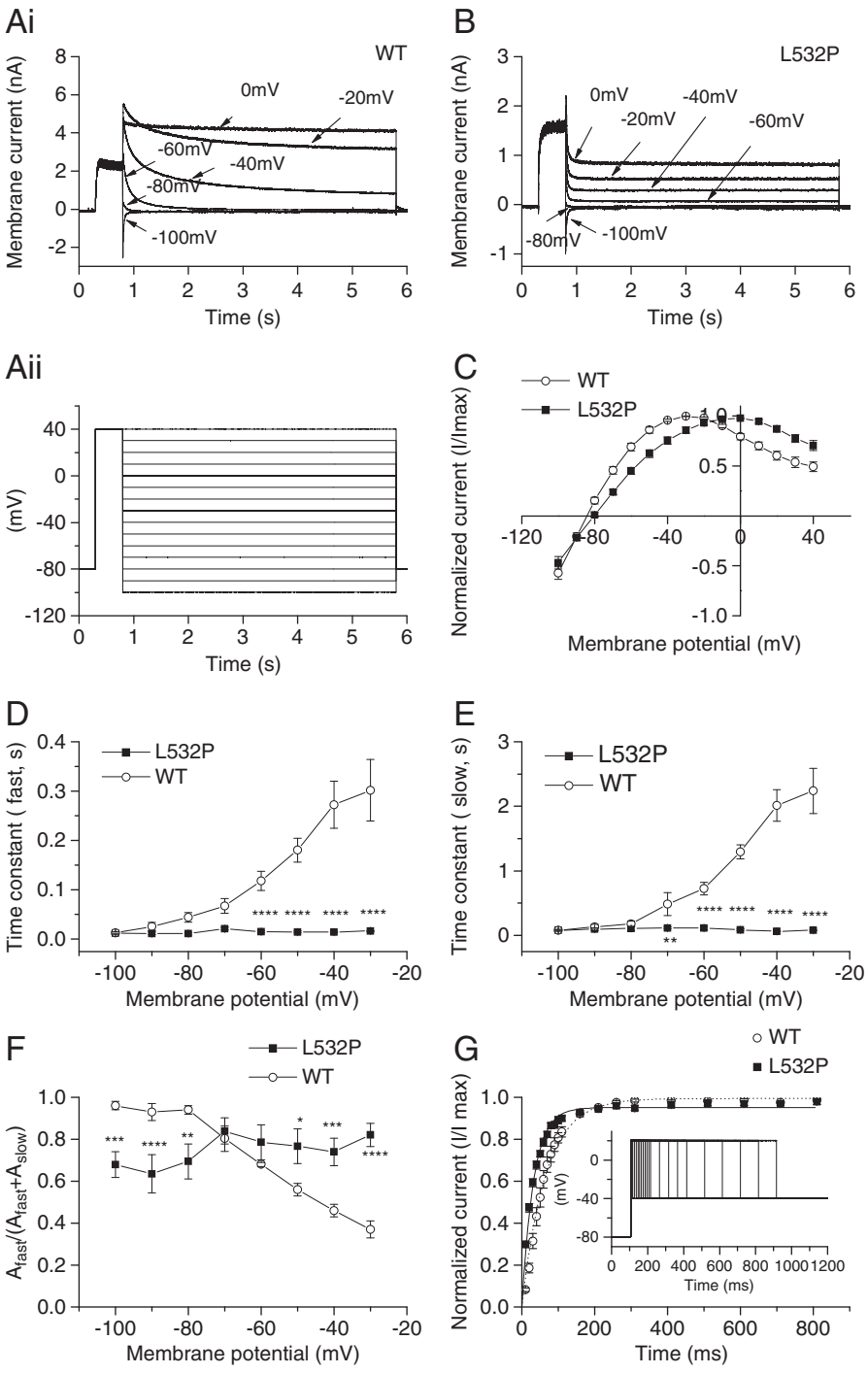

Fig. 3. Fully activated I–V relationships, I_{hERG} deactivation and activation time-course for WT and L532P. (Aii) Shows the protocol used to elicit the families of currents for WT I_{hERG} in Ai and for L532P I_{hERG} in B, from which the normalized fully activated I–V relations (C) were obtained (WT, n = 6; L532P, n = 9). In Ai and B selected currents are shown for clarity; note different current scales used. For 'C', peak I_{tails} at each repolarization potential were normalized to the peak outward I_{tail} during the protocol. (D, E) Fast and slow time-constants of deactivation from bi-exponential fits to the deactivating component of tail currents at each repolarization potential. (F) Plots of the proportion of fast deactivation against repolarization voltage in WT and L532P. (* denotes statistic significance of $P<0.05$, ** of $P\leq0.01$, *** of $P\leq0.005$, **** of $P\leq0.001$, for D–F, WT n = 6; L532P n = 9).(G) Activation time course of WT and L532P I_{hERG} at +20 mV elicited by an envelope of tails protocol shown in inset (WT n = 6; L532P n = 9).

and of 1.43 ± 0.12 ms for L532P (n = 11) ($P<0.005$). It should be noted that the greatly accelerated deactivation for L532P meant that after the first 2–3 current transients, the amplitude of successive transients declined. To highlight this, the plot in Fig. 4F also shows consecutive points for L532P joined by dotted straight lines. Collectively, the data shown in Fig. 4 indicate that the voltage-dependence of I_{hERG} inactivation was positively shifted (a $V_{0.5}$ shift of +32 mV), with a modest acceleration in recovery of inactivation.

Table 1 summarizes the biophysical parameters obtained for WT and L532P I_{hERG}

3.4. L532P I_{hERG} profile during ventricular AP clamp

An example trace of WT I_{hERG} during the course of an imposed ventricular AP waveform is shown in Fig. 5Ai, while Fig. 5Aii shows a comparable trace for L532P I_{hERG} (black trace, with the WT current

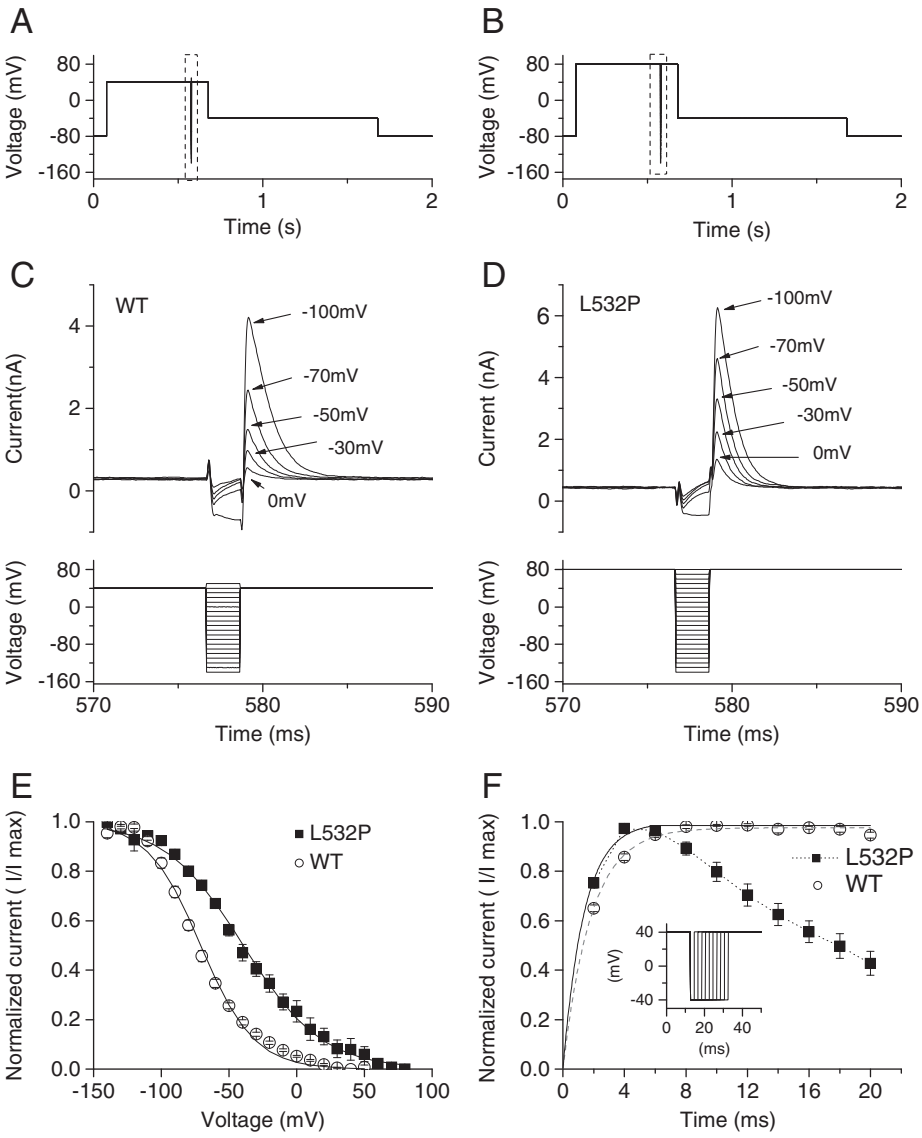

Fig. 4. Voltage and time-dependence of inactivation for WT and L532P. (A, B) show the voltage protocol used to determine the I_{hERG} availability for WT (A) and L532P (B) I_{hERG}. (C, D) Upper traces show representative records of WT and L532P I_{hERG} respectively, focusing on the current profile during the second and start of the third steps of the protocol as shown in lower panel. Note that the current scales in C and D differ. (E) I_{hERG} availability plots for WT (n = 9) and L532P (n = 8) hERG. (F) Recovery from inactivation time-course for WT and L532P hERG (protocol shown as inset). The dashed gray line denotes mono-exponential fit to WT data (n = 9). The solid line denotes mono-exponential fit to L532P data, with the dotted line connecting these data at successive time points (n = 8).

from Fig. 5Ai also overlaid (gray trace) for comparison). WT I_{hERG} increased progressively through the AP plateau phase, before declining during terminal AP repolarization (Fig. 5Ai and see [13,31,33]). By contrast, L532P I_{hERG} increased much earlier during the AP command, peaking earlier during the AP plateau phase, with a 'domed' or 'inverted U' shaped profile and more rapid decline than the WT current during the terminal AP phase (Fig. 5Aii). Fig. 5B shows the mean normalized instantaneous I–V relation for WT I_{hERG} during AP repolarization, with maximal current relatively late in repolarization (at -30.7 ± 2.1 mV; n = 7 cells). Fig. 5C shows the mean instantaneous I–V relation for L532P I_{hERG}, with current rising to a maximal value at $+15.7 \pm 2.4$ mV (n = 8; $P<0.0001$ versus WT) early in repolarization, then declining linearly with repolarization voltage

3.5. Modulation by L532P of pharmacological inhibition of I_{hERG} by dronedarone

Further experiments were performed in which effects were assessed of the L532P mutation on pharmacological inhibition of I_{hERG}. For these experiments, the Class III antiarrhythmic agent dronedarone (Droned) was chosen; this drug is a non-iodinated analog of amiodarone that exhibits hERG inhibition involving interaction with both activated and inactivated channels [29]. The voltage protocol used was composed of a 2 s voltage command to +20 mV, followed by repolarization to −40 mV to observe I_{hERG} tails. It also incorporated a brief (50 ms) pre-pulse from −80 to −40 mV prior to the test command, in order to quantify the instantaneous current at −40 mV. Comparison between this instantaneous current and the peak outward I_{hERG} tail amplitude on repolarization to −40 mV facilitated accurate measurement of WT I_{hERG} tail amplitude (cf [30,53]). For consistency the same protocol was applied in experiments on both WT and L532P I_{hERG}. Fig. 6A shows effects of 300 nM dronedarone on WT I_{hERG} while Fig. 6B shows comparable data for L532P I_{hERG}; current inhibition by the drug was more extensive for the WT than the mutant channel. Fig. 6C shows mean (run-down corrected) data for a range of drug concentrations, in which fractional block at each concentration plotted against the Log [Dronedarone] concentration. The data were fitted with a Hill equation and the derived IC_{50} and Hill co-efficient were 42.6 ± 3.4 nM and 0.9 ± 0.1 for

Table 1
Comparison of biophysical parameters for WT and L532P hERG.

Property	WT	L532P
$V_{act\ 0.5}$(mV)	−16.6 ± 2.3	19.2 ± 2.8
k (activation, mV)	6.8 ± 0.3 (n = 7 for both)	12.4 ± 0.9 (n = 9 for both)
τ_{act} (ms)	67.9 ± 6.1 (n = 9)	32.6 ± 2.2 (n = 6)
E_{rev} (mV)	−84.3 ± 0.9 (n = 6)	−80.3 ± 0.8 (n = 9)
$V_{inact0.5}$(mV)	−70.3 ± 1.7	−38.7 ± 3.7
k (inactivation,mV)	19.6 ± 0.5 (n = 9 for both)	28.7 ± 2.8 (n = 6 for both)
τ_{inact} (ms)	1.34 ± 0.13 (n = 9)	1.0 ± 0.06 (n = 6)
τ_{rec} (ms)	1.92 ± 0.07 (n = 10)	1.43 ± 0.12 (n = 11)

Abbreviations: $V_{act\ 0.5}$, half-maximal activation voltage; τ_{act}, time constant of activation; E_{rev}, reversal potential; $V_{inact0.5}$, half-maximal inactivation voltage; *k*, slope factor for activation or inactivation relationship; τ_{inact}, time constant of inactivation; τ_{rec}, time constant of recovery from inactivation; n = number of experimental replicates. Data are presented as mean ± s.e. mean.

WT hERG, and 227.0 ± 38.6 nM and 1.0 ± 0.2 for L532P hERG. Thus the L532P mutation resulted in a 5.3-fold rightward shift in the IC_{50} for I_{hERG} block by dronedarone ($P<0.005$ for WT and mutant IC_{50} values).

3.6. Homology modeling

In the absence of direct structural information from crystal structures of (h)ERG channels, homology modeling offers a useful way of investigating potential structural context(s) for changes to hERG channel function. Therefore, we adopted homology modeling based on a Kv1.2/2.1 template, in order to explore the structural context of the L532P mutation. The L532 residue resides in the helical S4 transmembrane segment, composed of ~20 amino acids as indicated by homology with eukaryotic voltage-gated channels of known structure (e.g. [45] and [50]). As shown in Fig. 1A, the amino acid sequence in this region is highly conserved, with positively charged residues (arginines or lysines) regularly separated by two hydrophobic residues. The hydrophobic leucine at residue 532 is located after the second arginine (R531) in the C-terminal half of S4 (Figs. 1A, 7A). The alignment of S4 (and adjacent sequence) between hERG and the Kv1.2/2.1 'paddle chimera' channel reported by Long et al [35], is shown in Fig. 7A. Homology modeling based on the paddle chimera (see Methods) places the L532 residue near the external face of the S4 helix where it lies close to the S5 helix of an adjacent subunit, at least in the open form of the channel model (Fig. 7B).

4. Discussion

4.1. Summary of principal findings

Although some characteristics of L532P I_{hERG} have been recorded at ambient temperature from channels expressed in *Xenopus* oocytes [25], to our knowledge there are no prior reports of similar data for mammalian cell hERG expression at 37 °C. Moreover, no information has hitherto been published on the effects of the L532P hERG mutation on time-dependent activation/inactivation kinetics of I_{hERG} or upon channel structure. Our data are in agreement with results obtained previously from *Xenopus* oocytes [25], in indicating a low activation threshold for L532P compared to WT I_{hERG}, with an accompanying shift in activation $V_{0.5}$ of ~+36 mV here compared to ~+41 mV in *Xenopus* oocytes [25]. However, a marked (~+50 mV) shift in voltage-dependent inactivation of L532P I_{hERG} from *Xenopus* oocytes was reported, whereas, under our experimental conditions the inactivation-shift produced by the mutation was somewhat less extensive (~+30 mV shift in $V_{0.5}$). In addition to these effects of the mutation on voltage-dependent kinetics of I_{hERG}, we also observed faster I_{hERG} activation (and deactivation) and faster recovery from

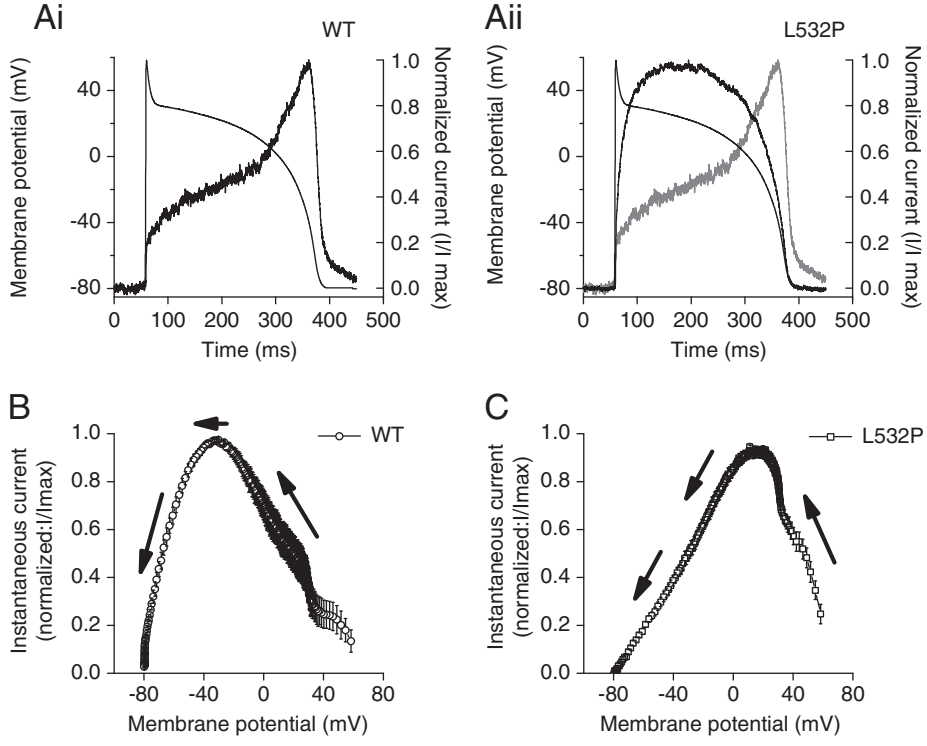

Fig. 5. I_{hERG} during ventricular action potential voltage-clamp (AP clamp) for WT and L532P hERG (Ai, Aii). Ventricular AP command waveform overlying I_{hERG} profiles for WT (Ai) and L532P (Aii). In Aii WT current profile is superimposed (in gray) on that for L532P current (black). For each of Ai and Aii, currents are normalized to peak current seen during the waveform (I/I_{max}). (B, C) Mean normalized plots of instantaneous current–voltage (I–V) relations for I_{hERG} during AP repolarization for WT (B; n = 7) and L532P (C; n = 8) I_{hERG}. The arrows indicate the direction of AP repolarization.

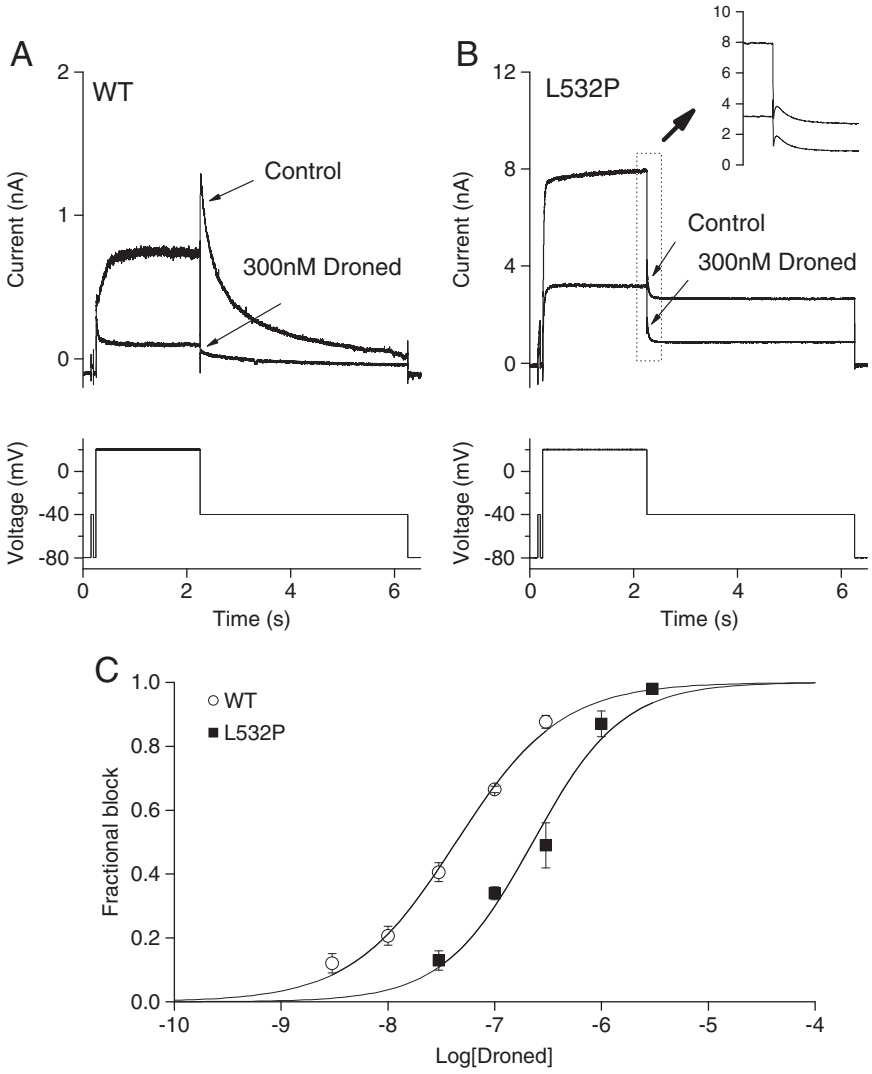

Fig. 6. Comparison of inhibition by dronedarone (Droned) of WT and L532P I_{hERG}. (A) Upper traces show WT I_{hERG} before and after 10 minute application of 300 nM Droned; protocol shown in lower trace. (B) Upper traces show L532P I_{hERG} before and after 10 minute application of 300 nM Droned, with an inset showing tail current on higher gain; lower trace shows voltage protocol. Note that the current scales in A and B differ. (C) Concentration–response relations for inhibition of WT and L532P I_{hERG} tails by Droned. At least five cells were used to test each drug concentration.

inactivation for L532P I_{hERG}. This combination of alterations results in a markedly altered current profile under AP voltage clamp (Fig. 5). We also provide the first demonstration that this S4 mutation, which is located in a region distinct from the S6 and inner helices that comprise the canonical drug binding site on hERG [2,36], has the potential to modify potency of drug block of I_{hERG}.

4.2. The L532P mutation in the context of S4 involvement in hERG channel gating

The hERG channel is distinguished by its rapid inactivation gating and comparatively slow activation gating. It is generally believed that slow activation of hERG starts from outward translation of the positive charged residues in S4 voltage sensor across the membrane field upon changes in membrane potential, which in turn causes opening of an activation gate involving S6 domains [28,37,41]. The S4–S5 linker has been suggested to couple directly S4 movement to the activation gate in hERG [38,39]. Alanine scanning mutagenesis and homology modeling have suggested a spiral pattern on the S4 domain of residues mutations to which perturb activation, with inactivation-perturbing mutation positions mapped to a distinct face of the S4 helix [38,45]. Positively charged residues K525, R528 and K538 in S4 have been suggested to be those most important for activation of the channel, with residues R528 and R531 as key candidates for binding to residues in other transmembrane domains through salt bridges and with residue R531 implicated in stabilizing the open state [42–44]. Alanine substitution at L532 produced little perturbation of activation or inactivation [45], whereas substitution with tryptophan (a bulkier hydrophobic residue) has been reported to accelerate deactivation rate, but to have comparatively little effect on activation rate [44]. The presence of proline residues in transmembrane helices of membrane proteins is well known to perturb helical structure [46]. Given this and the key role identified for residue R531 in activation gating, it is perhaps unsurprising that proline substitution at the adjacent L532 residue significantly alters I_{hERG} activation characteristics as it can be anticipated to alter S4 structure and influence of this domain on the S4–S5 linker. It has also been proposed that depolarization-induced motions in the S4 domain can change the orientation of 583–597 helix in the S5-P linker region of the channel or push it toward the pore, thereby facilitating I_{hERG} inactivation. Upon membrane repolarization, a reversal of the above S4 movements would occur [47]. Perturbation of the S4 helix by proline could influence such interactions and the modest but statistically significant shift in I_{hERG} reversal potential with the L532P-hERG is consistent with an allosteric effect of the mutation

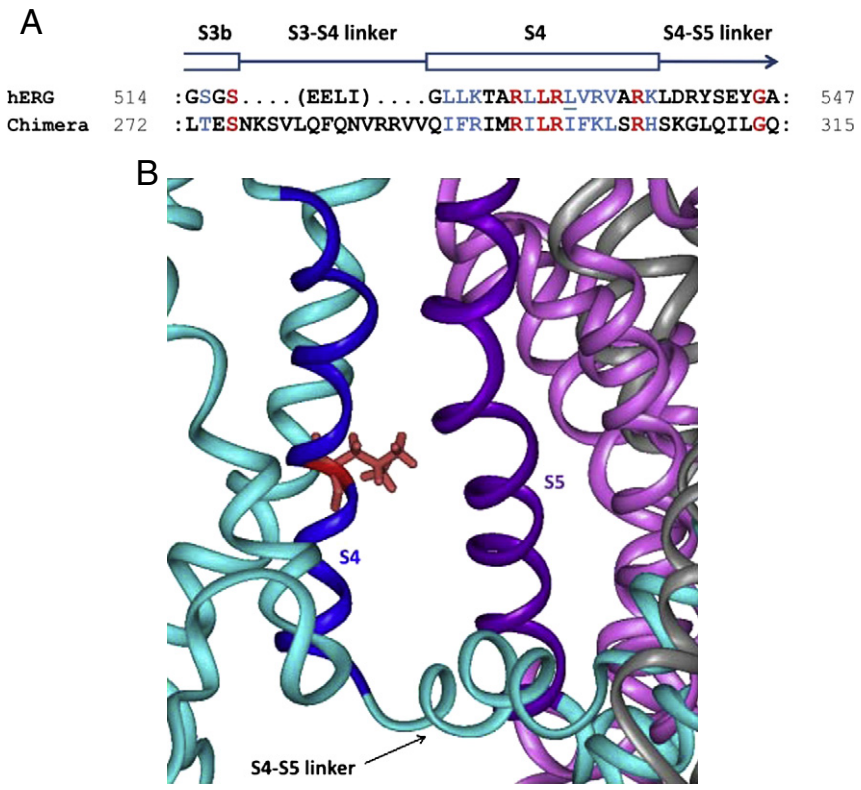

Fig. 7. Location of L532 in the context of the Kv1.2/2.1 chimera-based model of hERG. (A) Homology between hERG and the Kv1.2/2.1 chimera in and around the S4 sequence that was used for construction of this part of the hERG model. Amino acid identities are red; similarities are blue. The schematic above the sequences refers to the location of structural elements in the hERG model. (B) Close up of a hERG homology model based on the crystal structure of the Kv1.2/Kv2.1 paddle chimera, illustrating juxtaposition of the voltage sensor domain of one subunit (cyan/blue) with the pore domain of an adjacent subunit (pink/mauve). The L532 residue (red) in the S4 helix is oriented toward the S5 helix of an adjacent subunit.

on the channel's selectivity filter (the +4 mV shift in observed I_{hERG} reversal potential is consistent with a decrease in K^+ over Na^+ ion selectivity; equivalent to a P_{Na}/P_K ratio of ~1.6-fold that for WT hERG). Our homology modeling raises an additional possibility for the influence of the L532P mutation on channel gating and drug binding to side chains that line the permeation pathway (e.g. residues on S6). In the context of the model (Fig. 7B) residue L532 lies closely apposed to the S5 domain (lying opposite residues W568 and Y569 of the S5 domain of an adjacent hERG subunit, with a minimal distance between atoms of the apposing residues of ~3.5 Å). This raises the possibility of S4–S5 interactions that would be anticipated to differ between L532- and P532-containing channels; these might be transmitted to the S6 helix through the intimate interactions between S5 and S6 [51]. Given the comparative lack of effect of alanine substitution at L532 on activation/inactivation [45], one might speculate that, if present, these interactions become significant when a proline side chain is present in this residue. Further targeted mutagenesis work would be required to explore this possibility in greater depth.

4.3. Phenotype comparison with the N588K and T618I gain-of-function mutations

Under conditions comparable to those used in the present study, a previous investigation reported a marked (~+60 mV) voltage-shift in N588K I_{hERG} inactivation without any accompanying shift in activation [13]. The recently discovered T618I mutation has been reported to shift inactivation by ~+50 mV, with an additional ~−5 mV shift in activation. Thus, both of these human SQTS hERG mutations produce greater inactivation-shifts to that seen for L532P in the present study. There are no AP clamp data currently available for T618I hERG, but direct comparison is possible between our AP clamp data for L532P I_{hERG} and N588K I_{hERG} studied under similar conditions [13,14]. When elicited by a ventricular AP waveform similar to that used here, N588K I_{hERG} exhibited a similar dome-shaped current, with maximal current during repolarization occurring >60 mV positive to that for WT I_{hERG} [14]. Simulation data indicate that the altered timing and magnitude of repolarizing I_{Kr} in the setting of the SQT1 N588K mutation leads to marked ventricular AP abbreviation [17–19]. The AP abbreviation with N588K is also associated with flattening of the AP duration–restitution curve [18] and the overall effects of this mutation are likely to facilitate susceptibility to re-entrant arrhythmia. Despite differences from N588K-hERG in the overall effects on I_{hERG} kinetics of the L532P mutation, it resulted in a remarkably similar dome-shaped I_{hERG} profile under AP clamp to that seen for N588K-hERG, with an ~+47 mV shift in maximal outward current during repolarization. This is consistent with the previously advanced notion based on in silico modeling that kinetic changes produced by the L532P-hERG mutation could, in principle, lead to ventricular AP abbreviation [25]. In addition, the normally slow deactivation of I_{Kr}/I_{hERG} means that the underlying channels are able to conduct current for a period following completion of AP repolarization, which may normally confer some protection against premature depolarization [14,34,48]. Consistent with this, our AP clamp comparison of WT and L532P I_{hERG} (Fig. 5Aii) shows clearly that WT I_{hERG} had not yet returned fully to baseline immediately following completion of AP repolarization. By contrast, the overlain L532P current declines more extensively during this time (Fig. 5Aii) The marked acceleration of deactivation present for L532P-hERG might therefore be anticipated to impair the potentially protective effect of hERG and, if the mutation were to present clinically, this would likely increase ventricular susceptibility to premature excitation (although increased susceptibility to the effect of small magnitude premature depolarizations may be mitigated to some extent by the slight increase in window I_{hERG} negative to ~

−50 mV). As accelerated deactivation is a feature which is shared with L499P-zERG [25], it could have contributed to the increased arrhythmia susceptibility of *reg* mutant zebrafish [25].

The N588K-hERG mutation is well-established to attenuate markedly the inhibitory actions of Class III but not Class Ia antiarrhythmic drugs (which depend less than do Class III I_{Kr}-selective drugs on channel inactivation to bind) [10,15,16]. The T618I hERG mutation has been reported largely to retain sensitivity to inhibition by high concentrations of quinidine and sotalol, though full concentration–response data are not available [32]. The Class III agent dronedarone inhibits WT I_{hERG} in a manner that indicates contingency on channel gating, with little preference for activated over inactivated channel states [29]. The compound exhibits reduced I_{hERG} blocking potency under conditions of substantial inward [K^+] flux, which is suggestive of drug binding in or close to the ion conduction pathway [29]; docking analysis indicates that the compound can bind within the channel's inner cavity [40]. Considering this together with the location of the S4 domain relative to the inner cavity, it is unlikely that the L532 residue interacts directly with dronedarone. Rather, it is more likely that altered L532P-hERG channel gating impairs the ability of the drug to interact with its binding site. In this regard it is notable that the ~5-fold increase in IC_{50} for dronedarone seen here is similar to that (~4.2-fold) reported for structurally-related amiodarone with the N588K hERG mutation [30]. Indeed, the distinct location in the hERG channel of the N588, T618 and L532 residues, together with distinct kinetic effects of the N588K and L532P mutations under voltage clamp with similarities under AP clamp, makes the L532P mutant an attractive comparator for future pharmacological study targeted toward identifying consensus inhibitors of different known gain-of-function hERG mutants.

Acknowledgements

The authors thank Mrs Lesley Arberry for technical assistance, Dr Aziza El Harchi for statistical discussion and the British Heart Foundation for funding (grant numbers PG 06/042, and PG 10/017).

References

[1] J. Tamargo, R. Caballero, R. Gómez, C. Valenzuela, E. Delpón, Pharmacology of cardiac potassium channels, Cardiovasc. Res. 62 (2004) 9–33.
[2] J.C. Hancox, M.J. McPate, A. El Harchi, Y.H. Zhang, The hERG potassium channel and hERG screening for drug-induced torsades de pointes, Pharmacol. Ther. 119 (2008) 118–132.
[3] M.C. Sanguinetti, C. Jiang, M.E. Curran, M.T. Keating, A mechanistic link between an inherited and an acquired cardiac arrhythmia: HERG encodes the I_{Kr} potassium channel, Cell 81 (1995) 299–307.
[4] M.C. Trudeau, J.W. Warmke, B. Ganetzky, G.A. Robertson, HERG, an inward rectifier in the voltage-gated potassium channel family, Science 269 (1995) 92–95.
[5] S.M. Modell, M.H. Lehmann, The long QT syndrome family of cardiac ion channelopathies: a HuGE review, Genet. Med. 8 (2006) 143–155.
[6] M.C. Sanguinetti, M. Tristani-Firouzi, hERG potassium channels and cardiac arrhythmia, Nature 440 (2006) 463–469.
[7] M. Perry, M. Sanguinetti, J. Mitcheson, Revealing the structural basis of action of hERG potassium channel activators and blockers, J. Physiol. 588 (2010) 3157–3167.
[8] M.J. McPate, H.J. Witchel, J.C. Hancox, Short QT Syndrome, Futur. Cardiol. 2 (2006) 293–301.
[9] P. Maury, F. Extramiana, P. Sbragia, C. Giustetto, R. Schimpf, A. Duparc, C. Wolpert, I. Denjoy, M. Delay, M. Borgreffe, F. Gaita, Short QT syndrome. Update on a recent entity, Arch. Cardiovasc. Dis. 101 (2008) 779–786.
[10] R. Brugada, K. Hong, R. Dumaine, J. Cordeiro, F. Gaita, M. Borggrefe, T.M. Menendez, J. Brugada, G.D. Pollevick, C. Wolpert, E. Burashnikov, K. Matuso, Y.S. Wu, A. Guerchicoff, F. Bianchi, C. Guistetto, R. Schimpf, P. Brugada, C. Antzelevitch, Sudden death associated with short-QT syndrome linked to mutations in HERG, Circulation 109 (2004) 30–35.
[11] K. Hong, P. Bjeerregaard, I. Gussak, R. Brugada, Short QT syndrome and atrial fibrillation caused by mutation in KCNH2, J. Cardiovasc. Electophysiol. 16 (2005) 394–396.
[12] J.M. Cordeiro, R. Brugada, Y.S. Wu, K. Hong, R. Dumaine, Modulation of I_{Kr} inactivation by mutation N588K in KCNH2: a link to arrhythmogenesis in short QT syndrome, Cardiovasc. Res. 67 (2005) 498–509.
[13] M.J. McPate, R.S. Duncan, J.T. Milnes, H.J. Witchel, J.C. Hancox, The N588K-HERG K^+ channel mutation in the 'short QT syndrome': mechanism of gain-in-function determined at 37 °C, Biochem. Biophys. Res. Commun. 334 (2005) 441–449.
[14] M.J. McPate, H. Zhang, I. Ideniran, J.M. Cordeiro, H.J. Witchel, J.C. Hancox, Comparative effects of the short QT N588K mutation at 37 °C on hERG K^+ channel current during ventricular, Purkinje fibre and atrial action potentials: an action potential clamp study, J. Physiol. Pharmacol. 60 (2009) 23–41.
[15] C. Wolpert, R. Schimpf, C. Giustetto, C. Antzelevitch, J.M. Cordeiro, R. Dumaine, R. Brugada, K. Hong, U. Bauersfeld, F. Gaita, M. Borgreffe, Further insights into the effect of quinidine in short QT syndrome caused by a mutation in HERG, J. Cardiovasc. Electophysiol. 16 (2005) 54–58.
[16] M.J. McPate, R.S. Duncan, H.J. Witchel, J.C. Hancox, Disopyramide is an effective inhibitor of mutant HERG K^+ channels involved in variant 1 short QT syndrome, J. Mol. Cell. Cardiol. 41 (2006) 563–566.
[17] H. Zhang, J.C. Hancox, In silico study of action potential and QT interval shortening due to loss of inactivation of the cardiac rapid delayed rectifier potassium current, Biochem. Biophys. Res. Commun. 17 (2004) 693–699.
[18] S.G. Priori, S.V. Pandit, I. Rivolta, O. Berenfeld, E. Ronchetti, A. Dhamoon, C. Napolitano, J. Anumonwo, M.R. di Barletta, S. Gudapakkam, G. Bosi, M. Stramba-Badiale, J. Jalife, A novel form of short QT syndrome (SQT3) is caused by a mutation in the KCNJ2 gene, Circ. Res. 96 (2005) 800–807.
[19] D.L. Weiss, G. Seemann, F.B. Sachse, O. Dossel, Modelling of short QT syndrome in a heterogeneous model of the human ventricular wall, Europace 7 (2005) 105–117.
[20] H. Itoh, M. Horie, M. Ito, K. Imoto, Arrhythmogenesis in the short-QT syndrome associated with combined HERG channel gating defects: a simulation study, Circ. J. 70 (2006) 502–508.
[21] F. Extramiana, C. Antzelevitch, Amplified transmural dispersion of repolarization as the basis for arrhythmogenesis in a canine ventricular-wedge model of short-QT syndrome, Circulation 110 (2004) 3661–3666.
[22] C. Patel, C. Antzelevitch, Cellular basis for arrhythmogenesis in an experimental model of the SQT1 form of the short QT syndrome, Hear. Rhythm. 5 (2008) 585–590.
[23] P. Milberg, R. Tegelkamp, N. Osada, R. Schimpf, C. Wolpert, G. Breithardt, M. Borgreffe, L. Eckardt, Reduction of dispersion of repolarization and prolongation of postrepolarization refractoriness explain the antiarrhythmic effects of quinidine in a model of short QT syndrome, J. Cardiovasc. Electrophysiol. 18 (2007) 658–664.
[24] E. Nof, A. Burashnikov, C. Antzelevitch, Cellular basis for atrial fibrillation in an experimental model of short QT1: implications for a pharmacological approach to therapy, Hear. Rhythm. 7 (2010) 251–257.
[25] D. Hassel, E.P. Scholz, N. Trano, O. Friedrich, S. Just, B. Meder, D.L. Weiss, E. Zitron, S. Marquart, B. Vogel, C.A. Carle, G. Seemann, M.C. Fishman, H.A. Katus, W. Rottbauer, Deficient zebrafish ether-a-go-go-related gene channel gating causes short-QT syndrome in zebrafish reggae mutants, Circulation 117 (2008) 866–875.
[26] J.I. Vandenberg, A. Varghese, Y. Lu, J.A. Bursill, M.P. Mahaut-Smith, C.L. Huang, Temperature dependence of human ether-a-go-go-related gene K^+ currents, Am. J. Physiol. Cell. Physiol. 291 (2006) C165–C175.
[27] M. Weerapura, S. Nattel, D. Chartier, R. Caballero, T.F. Hebert, A comparison of currents carried by HERG with and without the coexpression of MiRP1, and the native rapid delayed rectifier current. Is MiRP1 the missing link? J. Physiol. 540 (2002) 15–27.
[28] S.B. Long, E.B. Campbell, R. MacKinnon, Voltage sensor of Kv1.2: structural basis of electromechanical coupling, Science 309 (2005) 903–908.
[29] J.M. Ridley, J.T. Milnes, H.J. Witchel, J.C. Hancox, High affinity HERG K^+ channel blockade by the antiarrhythmic agent dronedarone: resistance to mutations of the S6 residues Y652 and F656, Biochem. Biophys. Res. Commun. 325 (2004) 883–891.
[30] M.J. McPate, R.S. Duncan, J.C. Hancox, H.J. Witchel, Pharmacology of the short QT syndrome N588K-hERG K^+ channel mutation: differential impact on selected class I and class III antiarrhythmic drugs, Br. J. Pharmacol. 155 (2008) 957–966.
[31] J.C. Hancox, A.J. Levi, H.J. Witchel, Time course and voltage dependence of expressed HERG current compared with native 'rapid' delayed rectifier K current during the cardiac ventricular action potential, Pflugers Archiv. 436 (1998) 843–853.
[32] Y. Sun, X.Q. Quan, S. Fromme, R.H. Cox, P. Zhang, L. Zhang, D. Guo, J. Guo, C. Patel, P.R. Kowey, G.X. Yan, A novel mutation in the KCNH2 gene associated with short QT syndrome, J. Mol. Cell. Cardiol. 50 (2011) 433–441.
[33] Y.H. Zhang, H. Cheng, V.A. Alexeenko, C.E. Dempsey, J.C. Hancox, Characterization of recombinant hERG K^+ channel inhibition by the active metabolite of amiodarone desethyl-amiodarone, J. Electrocardiol. 43 (2010) 440–448.
[34] C.Y. Du, I. Adeniran, H. Cheng, Y.H. Zhang, A. El Harchi, M.J. McPate, H. Zhang, C.H. Orchard, J.C. Hancox, Acidosis impairs the protective role of hERG K^+ channels against premature stimulation, J. Cardiovasc. Electrophysiol. 21 (2010) 1160–1169.
[35] S.B. Long, X. Tao, E.B. Campbell, R. MacKinnon, Atomic structure of a voltage-dependent K^+ channel in a lipid membrane-like environment, Nature 450 (2007) 376–382.
[36] M.C. Sanguinetti, J.S. Mitcheson, Predicting drug-hERG channel interactions that cause acquired long QT syndrome, Trends Pharmacol. Sci. 26 (2005) 119–124.
[37] J.I. Vandenberg, A.M. Torres, T.J. Campbell, P.W. Kuchel, The HERG K^+ channel: progress in understanding the molecular basis of its unusual gating kinetics, Eur. Biophys. J. 33 (2004) 89–97.
[38] D.R. Piper, M.C. Sanguinetti, M. Tristani-Firouzi, Voltage sensor movement in the hERG K^+ channel, Novartis Found. Symp. 266 (2005) 46–52.

[39] T. Ferrer, J. Rupp, D.R. Piper, M. Tristani-Firouzi, The S4–S5 linker directly couples voltage sensor movement to the activation gate in the human Ether-à-go-go-related gene (hERG) K^+ channel, J. Biol. Chem. 281 (2006) 12858–12864.
[40] P.J. Stansfeld, P. Gedeck, M. Gosling, B. Cox, J.S. Mitcheson, M.J. Sutcliffe, Drug block of the hERG potassium channel: insight from modeling, Proteins 68 (2007) 568–580.
[41] M.C. Sanguinetti, M. Tristani-Firouzi, hERG potassium channels and cardiac arrhythmia, Nature 440 (2006) 463–469.
[42] M. Zhang, J. Liu, G.N. Tseng, Gating charges in the activation and inactivation processes of the HERG channel, J. General Physiol. 124 (2004) 703–718.
[43] R.N. Subbiah, C.E. Clarke, D.J. Smith, J.T. Zhao, T.J. Campbell, J.I. Vandenberg, Molecular basis of slow activation of the human ether-á-go-go related gene potassium channel, J. Physiol. 558 (2004) 417–431.
[44] R.N. Subbiah, M. Kondo, T.J. Campbell, J.I. Vandenberg, Tryptophan scanning mutagenesis of the HERG K^+ channel: the S4 domain is loosely packed and likely to be lipid exposed, J. Physiol. 569 (2005) 367–379.
[45] D.R. Piper, W.A. Hinz, C.K. Tallurri, M.C. Sanguinetti, M. Tristani-Firouzi, Regional specificity of human ether-a-go-go-related gene channel activation and inactivation gating, J. Biol. Chem. 280 (2005) 7206–7217.
[46] M.S. Sansom, H. Weinstein, Hinges, swivels and switches: the role of prolines in signalling via transmembrane alpha-helices, Trends Pharmacol. Sci. 21 (2000) 445–451.
[47] J. Liu, M. Zhang, M. Jiang, G.N. Tseng, Structural and functional role of the extracellular S5-P linker in the HERG potassium channel, J. Gen. Physiol. 120 (2002) 723–737.
[48] Y. Lu, M.P. Mahaut-Smith, A. Varghese, C.L. Huang, P.R. Kemp, J.I. Vandenberg, Effects of premature stimulation on HERG K^+ channels, J. Physiol. 537 (2001) 843–851.
[49] R.A. Laskowski, M.W. MacArthur, D.S. Moss, J.M. Thornton, PROCHECK: a program to check the stereochemical quality of protein structure, J. Appl. Cryst. 26 (1993) 283–291.
[50] S.Y. Lee, A. Banerjee, R. MacKinnon, Two separate interfaces between the voltage sensor and pore are required for the function of voltage-dependent K^+ channels, PLoS Biol. 7 (2009) e1000047.
[51] P. Ju, G. Pages, R.P. Riek, P. Chen, A.M. Torres, P.S. Bansal, S. Kuyucak, P.W. Kuchel, J.I. Vandenberg, The pore domain outer helix contributes to both activation and inactivation of the HERG K^+ channel, J. Biol. Chem. 284 (2009) 1000–1008.
[52] A. Zou, Q.P. Xu, M.C. Sanguinetti, A mutation in the pore region of HERG K^+ channels expressed in *Xenopus* oocytes reduces rectification by shifting the voltage dependence of inactivation, J. Physiol. 509 (1998) 129–137.
[53] R.S. Duncan, M.J. McPate, J.M. Ridley, Z. Gao, A.F. James, D.J. Leishman, J.L. Leaney, H.J. Witchel, J.C. Hancox, Inhibition of the HERG potassium channel by the tricyclic antidepressant doxepin, Biochem. Pharmacol. 74 (2007) 425–437.